Strain-tunable magnetocrystalline anisotropy in epitaxial $Y_3Fe_5O_{12}$ thin films

Hailong Wang,* Chunhui Du,* P. Chris Hammel,† and Fengyuan Yang†
Department of Physics, The Ohio State University, Columbus, Ohio 43210, USA
(Received 6 December 2013; revised manuscript received 20 February 2014; published 7 April 2014)

We demonstrate strain tuning of magnetocrystalline anisotropy over a range of more than 1000 G in epitaxial $Y_3Fe_5O_{12}$ films of excellent crystalline quality grown on lattice-mismatched $Y_3Al_5O_{12}$ substrates. Ferromagnetic resonance (FMR) measurements reveal a linear dependence of both out-of-plane and in-plane uniaxial anisotropy on the strain-induced tetragonal distortion of $Y_3Fe_5O_{12}$. Importantly, we find the spin mixing conductance G_r determined from inverse spin Hall effect and FMR linewidth broadening remains large: $G_r = 3.33 \times 10^{14}\ \Omega^{-1}\,m^{-2}$ in $Pt/Y_3Fe_5O_{12}/Y_3Al_5O_{12}$ heterostructures, quite comparable to the value found in $Pt/Y_3Fe_5O_{12}$ grown on lattice-matched $Gd_3Ga_5O_{12}$ substrates.

DOI: 10.1103/PhysRevB.89.134404 PACS number(s): 75.30.Gw, 75.70.Tj, 76.50.+g, 81.15.−z

Magnetocrystalline anisotropy (MCA) [1–6] plays an essential role in various applications such as permanent magnets and magnetic data storage. There is intense interest in understanding the role of magnetoelastic coupling in phonon-magnon interactions in thermal spintronics. It is important to understand MCA in the presence of lattice distortion induced by epitaxial strain and the underlying magnetization-lattice coupling. Tunable magnetic anisotropy was observed in GaMnAs [3], GaMnAsP [4], and Sr_2FeMoO_6 [6] epitaxial films. $Y_3Fe_5O_{12}$ (YIG) is widely used in FMR and microwave applications as well as spin dynamics studies [7–11] due to its exceptionally low damping. Most YIG epitaxial films and single crystals are produced by liquid-phase epitaxy (LPE) [12]. Pulsed-laser deposition (PLD) has also been used to grow YIG thin films [13–15]. However, a systematic study of strain dependence of MCA is lacking, largely due to the challenge in controlling the epitaxial strain while maintaining high crystalline quality. Strain control in high quality YIG films will allow tuning of MCA, which in turn determines the static and dynamic magnetization of the YIG films.

Most reported YIG epitaxial film fabrication has employed $Gd_3Ga_5O_{12}$ (GGG) substrates which has a lattice mismatch $\eta = (a_s - a_f)/a_f \times 100\%$ of 0.057% with YIG, where $a_s = 12.383$ Å and $a_f = 12.376$ Å are the lattice constants of the GGG substrate and unstrained YIG, respectively. In order to probe the MCA in epitaxial YIG films in response to lattice distortion, we report in this article the growth of YIG epitaxial thin films on (001)-oriented $Y_3Al_5O_{12}$ (YAG) substrate [12,16,17] with $a_s = 12.003$ Å ($\eta = -3.0\%$). The larger lattice mismatch results in thickness-controlled strain-induced tetragonal distortion in the YIG films, which leads to variation in their out-of-plane and in-plane MCA as discussed below.

We grow epitaxial YIG films with thicknesses t ranging from 9.8 to 72.7 nm using a new sputtering technique [10,11,18,19] on YAG (001) substrates and determine their crystalline quality by triple-axis x-ray diffraction (XRD). Figure 1(a) shows 2θ-ω XRD scans of the YIG films of seven different thicknesses on YAG (001). The pronounced Laue oscillations observed in the 37.9- and 72.7-nm films indicate smooth surfaces and sharp YIG/YAG interfaces. The atomic force microscopy (AFM) images in Figs. 1(c) and 1(d) for the 9.8- and 72.7-nm YIG films show a root-mean-square (rms) roughness of 0.17 and 0.16 nm, respectively, indicating that our films have smooth surfaces with similar roughness. The gradual shift of the YIG (004) peak position reflects strain relaxation as the film thickness increases. The lattice mismatch (−3.0%, compressive) elongates the out-of-plane lattice constant c, resulting in a tetragonal distortion. To obtain the in-plane lattice constant a, we assume conservation of the unit cell volume of YIG during strain relaxation, $a = \sqrt{(12.376\ \text{Å})^3/c}$. Figure 1(b) and Table I show the values of a and c for all the YIG films, which exhibit a clear strain relaxation as t increases, while the strain-induced tetragonal distortion $\sigma = (c - a)/a$ of the films decreases from 2.05% to 0.073%.

We determine the magnetic anisotropy of our YIG films using FMR spectroscopy at radio frequency (rf) $f = 9.60$ GHz in a cavity. A magnetic field $\boldsymbol{H}$ is applied at an angle θ_H with respect to the film normal [see inset to Fig. 2(a)]. Figure 2(a) shows four representative FMR spectra for the 72.7-nm YIG film at $\theta_H = 0°$, 30°, 50°, and 90°. The resonance field H_{res} is defined as the field at which the derivative of the FMR absorption crosses zero. Figure 2(b) shows the angular (θ_H) dependence of H_{res} for the 9.8-, 15.0-, 29.3-, and 72.7-nm YIG films as σ varies from 2.05% to 0.073%. The magnetization can be quantitatively characterized from the total free energy density F for the YIG films with tetragonal symmetry [20,21],

$$F = -\boldsymbol{H}\cdot\boldsymbol{M} + \frac{1}{2}M\left\{4\pi M_{\text{eff}}\cos^2\theta - \frac{1}{2}H_{4\perp}\cos^4\theta - \frac{1}{8}H_{4||}(3+\cos4\phi)\sin^4\theta - H_{2||}\sin^2\theta\sin^2\left(\phi-\frac{\pi}{4}\right)\right\}, \quad (1)$$

where θ and ϕ are angles describing the orientation of the equilibrium magnetization ($\boldsymbol{M}$) [see inset to Fig. 2(a)]. The first term in Eq. (1) is the Zeeman energy and the second term is the effective demagnetizing energy $4\pi M_{\text{eff}} = 4\pi M_s - H_{2\perp}$ which includes the shape anisotropy ($4\pi M_s$)

*These authors made equal contributions to this work.
†Corresponding authors: hammel@physics.osu.edu; fyyang@physics.osu.edu

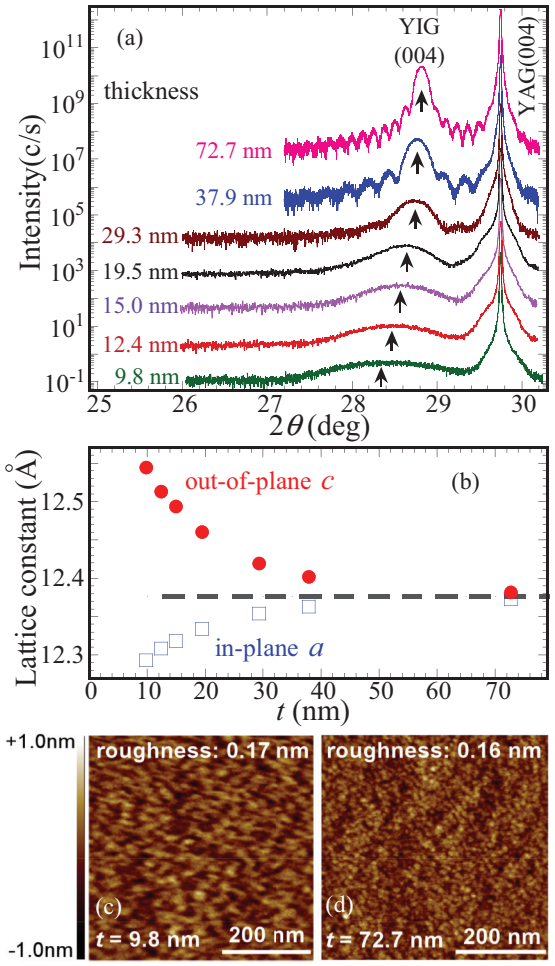

FIG. 1. (Color online) (a) Semilog 2θ-ω XRD scans of YIG films of thickness $t = 9.8$, 12.4, 15.0, 19.5, 29.3, 37.9, and 72.7 nm grown on YAG (001) substrates. The arrows indicate the positions of the YIG (004) peak. The satellite peaks in the scans of 37.9- and 72.7-nm YIG films are the Laue oscillations. (b) Thickness dependence of the in-plane (blue open squares) lattice constant a and out-of-plane (red solid circles) lattice constant c of the YIG films on YAG. The horizontal dashed line represents the bulk lattice constant $a = 12.376$ Å of YIG. AFM images of (c) 9.8-nm and (d) 72.7-nm YIG films on YAG with rms roughness of 0.17 and 0.16 nm, respectively.

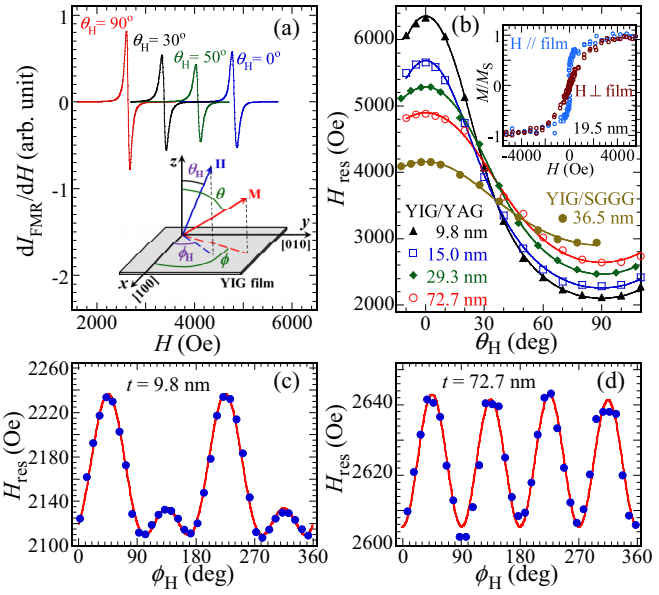

FIG. 2. (Color online) (a) Room-temperature FMR derivative spectra for a 72.7-nm YIG film on YAG (001) at $\theta_H = 0°$, 30°, 50°, and 90°. Inset: Coordinate system used for FMR measurements and analysis. (b) Out-of-plane angular dependence (θ_H) of the resonance fields (H_{res}) for the 9.8-, 15.0-, 29.3-, and 72.7-nm YIG films on YAG (100) and a 36.5-nm YIG film on SGGG (111). The fitting (solid curves) was performed using Eqs. (1) and (2) to obtain $4\pi M_{eff}$, from which $H_{2\perp}$ was determined for each film. Inset: In-plane (blue) and out-of-plane (red) magnetic hysteresis loops of a 19.5-nm thick YIG film. In-plane angular dependence (ϕ_H) of H_{res} for the (c) 9.8-nm and (d) 72.7-nm YIG films.

and out-of-plane uniaxial anisotropy $H_{2\perp}$. The remaining terms are out-of-plane cubic anisotropy ($H_{4\perp}$), in-plane cubic anisotropy ($H_{4||}$), and in-plane uniaxial anisotropy ($H_{2||}$).

We measure the magnetic hysteresis loops of the YIG films using a vibrating sample magnetometer (VSM) to obtain the saturation magnetization M_s. The values of $4\pi M_s$ vary from 1590 ± 32 to 1851 ± 37 Oe, which lie in the range of reported magnetization in YIG samples grown by LPE and PLD [12–15,22]. The inset to Fig. 2(b) shows representative in-plane and out-of-plane hysteresis loops for the 19.5-nm YIG film, indicating clear magnetic shape anisotropy. Due to strain relaxation, the coercivity of our YIG films on YAG (001) ranges from 30 to 80 Oe for different thicknesses, much larger than the values of YIG films on lattice-matched GGG [14].

The equilibrium orientation (θ, ϕ) of magnetization can be obtained by minimizing the free energy, and the FMR

TABLE I. Structural and magnetic parameters of YIG epitaxial films with thickness $9.8 \le t \le 72.7$ nm on YAG (001) and a 36.5-nm YIG film (*italic*) on SGGG (111).

t (nm)	a (Å)	c (Å)	$(c-a)/a$	$4\pi M_s$ (Oe)	$4\pi M_{eff}$ (Oe)	$H_{2\perp}$ (Oe)	E_{ani} (10^3 erg/cm^3)	$H_{2\|\|}$ (Oe)	$H_{4\|\|}$ (Oe)
9.8	12.293	12.545	2.05%	1851 ± 37	3103 ± 62	−1252 ± 25	92.2 ± 3.7	60.4 ± 1.2	42.0 ± 1.2
12.4	12.308	12.513	1.66%	1756 ± 35	2658 ± 53	−902 ± 18	63.0 ± 3.7	48.7 ± 1.0	58.6 ± 1.2
15.0	12.318	12.493	1.43%	1640 ± 33	2341 ± 47	−701 ± 14	45.7 ± 1.8	52.1 ± 1.0	66.8 ± 1.3
19.5	12.334	12.460	1.03%	1745 ± 46	2289 ± 46	−543 ± 11	37.7 ± 1.5	17.9 ± 0.4	17.9 ± 0.4
29.3	12.354	12.420	0.53%	1644 ± 33	2088 ± 42	−445 ± 8.9	29.1 ± 1.2	23.9 ± 0.5	18.0 ± 0.4
37.9	12.363	12.402	0.31%	1806 ± 36	1945 ± 39	−139 ± 2.8	10.0 ± 0.40	2.75 ± 0.1	25.9 ± 0.5
72.7	12.373	12.382	0.073%	1590 ± 32	1639 ± 33	−49 ± 1.0	3.10 ± 0.12	0.941 ± 0.02	25.6 ± 0.5
36.5	*12.416*	*12.297*	*−0.96%*	*1606 ± 32*	*857 ± 17*	*+749 ± 15*	*−47.9 ± 1.9*		

resonance frequency ω in equilibrium is given by [20,21,23]

$$\left(\frac{\omega}{\gamma}\right)^2 = \frac{1}{M^2\sin^2\theta}\left[\frac{\partial^2 F}{\partial\theta^2}\frac{\partial^2 F}{\partial\phi^2} - \left(\frac{\partial^2 F}{\partial\theta\partial\phi}\right)^2\right], \quad (2)$$

where γ is the gyromagnetic ratio. We use a numerical procedure to obtain the equilibrium angles at resonance condition [24,25] and fit the $H_{\rm res}$ vs $\theta_{\rm H}$ data to determine $4\pi M_{\rm eff}$, $H_{4\perp}$, $H_{4||}$, $H_{2||}$, and g factor. In Fig. 2(b) the fitting curves agree well with the experimental data which reveal a systematic variation of $4\pi M_{\rm eff}$ for YIG films of different thicknesses. For the 9.8-nm film, $4\pi M_{\rm eff} = 3103 \pm 62$ Oe, while for the 72.7-nm film, $4\pi M_{\rm eff} = 1639 \pm 33$ Oe, indicating that the strain induces substantial out-of-plane anisotropy $H_{2\perp}$ (Table I), which can be calculated from the values of $M_{\rm s}$ and $4\pi M_{\rm eff}$. We also find that the in-plane uniaxial anisotropy $H_{2||}$ increases with tetragonality of the YIG lattice. Figures 2(c) and 2(d) show both the experimental data and fits to the in-plane angular dependence of $H_{\rm res}$ for the 9.8- and 72.7-nm YIG films on YAG. Clear fourfold symmetry is observed in the 72.7-nm YIG film, while superposition of two- and fourfold symmetry appears in the 9.8-nm YIG film, from which the in-plane cubic ($H_{4||}$) and uniaxial ($H_{2||}$) anisotropy can be obtained using [20,21]

$$\left(\frac{\omega}{\gamma}\right)^2 = \left\{H + H_{4||}\cos 4\phi - H_{2||}\cos\left(2\phi - \frac{\pi}{2}\right)\right\}\left\{H + 4\pi M_{\rm eff} + \frac{H_{4||}(3+\cos 4\phi)}{4} + H_{2||}\sin^2\left(\phi - \frac{\pi}{4}\right)\right\}. \quad (3)$$

Figure 3(a) shows $H_{2\perp}$ as a function of σ for all the YIG films on YAG; $H_{2\perp}$ varies linearly with strain. This tunability of MCA through lattice symmetry highlights the central result of our study: the proportionality of $H_{2\perp}$ to the tetragonal distortion of the YIG lattice over a broad range [$-2.05\% < (c-a)/a < -0.073\%$]: $H_{2\perp} = (12 \pm 64) - (55.8 \pm 5.3)10^3[(c-a)/a]$ (Oe). The linear relationship between MCA and lattice symmetry is expected but has not been seen before in YIG films. In order to verify that the large strain-induced $H_{2\perp}$ in YIG/YAG exists not just in YIG films with compressive strain, we also deposited YIG films on (111)-oriented substituted-$Gd_3Ga_5O_{12}$ (SGGG) substrate with a lattice constant $a_{\rm s} = 12.505$ Å which produces a +1.04% tensile strain. The fitting to the data of a 36.5-nm YIG film on SGGG in Fig. 2(b) gives $4\pi M_{\rm eff} = 857 \pm 17$ Oe, from which we obtain $H_{2\perp} = +749 \pm 15$ Oe using $4\pi M_{\rm s} = 1606 \pm 32$ Oe. The positive sign of this $H_{2\perp}$ arises from the expanded $a = 12.416$ Å and compressed $c = 12.297$ Å, which is opposite to those for YIG/YAG. This result confirms that the strain-induced uniaxial anisotropy arises from the tetragonal distortion of the YIG lattice and opposite strains produce opposite signs of $H_{2\perp}$. Figure 3(b) plots the dependence of $H_{2||}$ on $(c-a)/a$, where $H_{2||}$ decreases from 60.4 to 0.941 Oe as the tetragonality is reduced from 2.05% (9.8-nm film) to 0.073% (72.7-nm film). A linear fit to Fig. 3(b) gives $H_{2||} = (2 \pm 6) + (31.1 \pm 4.6)10^2[(c-a)/a]$ (Oe).

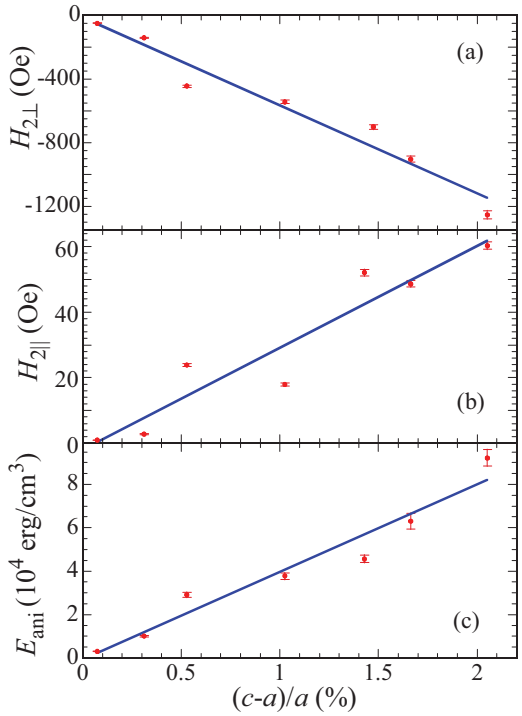

FIG. 3. (Color online) (a) Out-of-plane uniaxial anisotropy field $H_{2\perp}$, (b) in-plane anisotropy field $H_{2||}$, and (c) out-of-plane anisotropy energy $E_{\rm ani}$ as a function of the tetragonal distortion $(c-a)/a$ of the YIG films on YAG.

For cubic systems like garnets, epitaxial strain induces an out-of-plane tetragonal distortion of the lattice, while the two in-plane axes should be equivalent. This should lead to an out-of-plane uniaxial anisotropy, while an in-plane uniaxial anisotropy is not expected. However, in-plane uniaxial anisotropy has been experimentally observed in various magnetic epitaxial films with cubic structure, such as Fe and Co_2MnGe films on GaAs (001) [26,27] and $Co_2FeAl_{0.5}Si_{0.5}$ films on $MgAl_2O_4$ (001) [28], similar to our YIG films on YAG (001). One notes that the in-plane uniaxial anisotropy exists only in strained YIG films with tetragonal distortion and essentially disappears when the films are fully relaxed (e.g., the 72.7-nm film). While both of strain-induced and interfacial anisotropy are possible, the specific mechanisms for the observed in-plane uniaxial anisotropy are an open question.

The measured in-plane cubic anisotropy $H_{4||}$ (Table I) does not exhibit a systematic dependence on film thickness or tetragonal distortion, which indicates that $H_{4||}$ is not sensitive to strain in YIG and its magnitude is much smaller than $H_{2\perp}$. Here we mainly focus on the out-of-plane uniaxial anisotropy given its dominant role in strain-induced anisotropy.

The strain-induced $H_{2\perp}$ arises from magnetization-lattice coupling [29,30] in which a change in interatomic distances alters the magnetic properties through spin-orbit coupling. The magnetoelastic energy density is given by $F = -\sigma b$ when $\boldsymbol{M}$ is along the [001] direction, where b and σ are

the magnetoelastic constant and tetragonality $(c - a)/a$, respectively. Figure 3(c) shows the linear dependence of the out-of-plane uniaxial anisotropy energy $E_{\text{ani}} = -\frac{1}{2}MH_{2\perp}$ on σ for all the YIG films on YAG. A least squares fit in Fig. 3(c) gives $E_{\text{ani}} = (-7.0 \pm 54.2) \times 10^2 + (40.4 \pm 4.4) \times 10^5[(c - a)/a]$ (erg/cm^3), from which we obtain $-b = (40.4 \pm 4.4) \times 10^5$ erg/cm^3. The negative value of b implies that the magnetic easy axis is parallel to a short axis of the tetragonal lattice. The magnetoelastic constant of YIG is somewhat smaller than but of the same order as that in double perovskite Sr_2FeMoO_6 films with $-b = (92.9 \pm 4.5) \times 10^5$ erg/cm^3 [6]. The similarity may arise because both $Y_3Fe_5O_{12}$ and Sr_2FeMoO_6 are Fe^{3+}-based ferrimagnetic oxides, while the presence of 4d transition metal Mo^{5+} in Sr_2FeMoO_6 enhances the spin-orbit coupling and, consequently, the magnetoelastic coupling. This result demonstrates the ability to tune MCA in thin YIG epitaxial films by substrate lattice mismatch and film thickness.

FMR driven spin pumping of a pure spin current from a ferromagnet (such as YIG) to a nonmagnetic material is a powerful technique for probing the quality of the ferromagnetic films and their surfaces [7]. Due to the exceptionally low magnetic damping and insulating nature, YIG has been regarded as an ideal material for FMR spin pumping. One key question here is the effect of strain in YIG films on spin pumping. This is particularly interesting given YIG's narrow linewidth which determines the precession cone angle of the YIG magnetization and strongly influences spin transfer. Hence it is important to understand strain-induced FMR linewidth broadening in YIG/YAG films [9,10]. It is generally believed that the FMR linewidth reflects the quality of YIG films, and large linewidth implies poor quality. However, we find that in spite of the large linewidths in YIG films on YAG which we believe arise from strain-induced defects in the bulk of the films, the spin mixing conductance of the interface remains high. Figure 4(a) shows the spin pumping result of a Pt(5 nm)/YIG(72.7 nm) bilayer on YAG with an inverse spin Hall effect (ISHE) voltage (V_{ISHE}) of 123 μV which, although smaller than our previously reported mV-level V_{ISHE} for Pt/YIG on GGG [10], is still large for the Pt/YIG system. Figure 4(b) shows the FMR derivative absorption spectra of a single 72.7-nm YIG film and the Pt(5 nm)/YIG(72.7 nm) bilayer on YAG. The real part of spin mixing conductance G_r can be determined from the line broadening [31,32]; we observe the linewidth to increase from 83.9 to 88.9 Oe after the deposition of Pt on YIG,

$$G_r = \frac{e^2}{h}\frac{2\sqrt{3}\pi M_s \gamma t_F}{g\mu_B \omega}(\Delta H_{\text{Pt/YIG}} - \Delta H_{\text{YIG}}), \qquad (4)$$

where g, μ_B, and t_F are the Landé g factor, Bohr magneton, and thickness of YIG film, respectively. Using Eq. (4) and the linewidths from Fig. 4(b), we obtain the spin mixing conductance $(3.33 \pm 0.15) \times 10^{14}$ Ω^{-1} m^{-2} for Pt/YIG on YAG, which is slightly smaller but comparable to the values of $(3.73 \pm 0.17) \times 10^{14}$ and $(4.56 \pm 0.21) \times 10^{14}$ Ω^{-1} m^{-2} for Pt/YIG bilayers on GGG [10]. This indicates that though the FMR linewidth for YIG films grown on YAG is larger, the interfacial spin mixing conductance remains high, implying that while the strain-induced inhomogeneity suppresses the global precession of magnetization in the bulk of the YIG film, the spin mixing conductance relies on the local Pt/YIG interfacial characteristics.

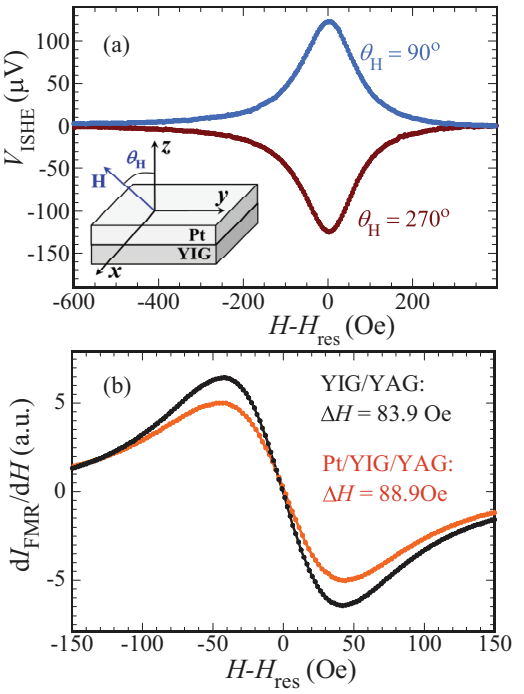

FIG. 4. (Color online) (a) V_{ISHE} vs H spectra at $\theta_H = 90°$ and 270° using $P_{\text{rf}} = 200$ mW for a Pt(5 nm)/YIG(72.7 nm) bilayer. Inset: FMR spin pumping experimental geometry. (b) FMR derivative absorption spectra of the 72.7-nm thick YIG film before (red) and after (blue) the deposition of a 5-nm Pt layer.

In summary, tunable magnetocrystalline anisotropy in strained YIG thin films shows a clear linear dependence on the tetragonal distortion of YIG lattice. This provides insights into magnetization-lattice coupling in this important magnetic material and could enable potential microwave and spin-electronic applications via control of the lattice symmetry. In particular, this suggests microwave heterostructures that employ strain engineering of YIG epitaxial films via lateral strain modulation to tune magnetic resonance characteristics for applications.

This work is supported by the Center for Emergent Materials at the Ohio State University, a NSF Materials Research Science and Engineering Center (DMR-0820414) (H.L.W. and F.Y.Y.) and by the Department of Energy through Grant DE-FG02-03ER46054 (P.C.H.). Partial support is provided by Lake Shore Cryogenics Inc. (C.H.D.) and the NanoSystems Laboratory at the Ohio State University.

[1] B. Heinrich, K. B. Urquhart, A. S. Arrott, J. F. Cochran, K. Myrtle, and S. T. Purcell, Phys. Rev. Lett. **59**, 1756 (1987).

[2] M. Kowalewski, C. M. Schneider, and B. Heinrich, Phys. Rev. B **47**, 8748 (1993).

[3] S. H. Kim, H. K. Lee, T. H. Yoo, S. Y. Lee, S. H. Lee, X. Liu, and J. K. Furdyna, J. Appl. Phys. **107**, 103911 (2010).
[4] M. Cubukcu, H. J. von Bardeleben, Kh. Khazen, J. L. Cantin, O. Mauguin, L. Largeau, and A. Lemaître, Phys. Rev. B **81**, 041202(R) (2010).
[5] C. Kwon, S. E. Lofland, S. M. Bhagat, M. Rajeswari, T. Venkatesan, R. Ramesh, A. R. Kratz, and R. D. Gomez, IEEE Trans. Magn. **33**, 3964 (1997).
[6] C. H. Du, R. Adur, H. L. Wang, A. J. Hauser, F. Y. Yang, and P. C. Hammel, Phys. Rev. Lett. **110**, 147204 (2013).
[7] Y. Kajiwara, K. Harii, S. Takahashi, J. Ohe, K. Uchida, M. Mizuguchi, H. Umezawa, H. Kawai, K. Ando, K. Takanashi, S. Maekawa, and E. Saitoh, Nature (London) **464**, 262 (2010).
[8] C. W. Sandweg, Y. Kajiwara, A. V. Chumak, A. A. Serga, V. I. Vasyuchka, M. B. Jungfleisch, E. Saitoh, and B. Hillebrands, Phys. Rev. Lett. **106**, 216601 (2011).
[9] B. Heinrich, C. Burrowes, E. Montoya, B. Kardasz, E. Girt, Y.-Y. Song, Y. Y. Sun, and M. Z. Wu, Phys. Rev. Lett. **107**, 066604 (2011).
[10] H. L. Wang, C. H. Du, Y. Pu, R. Adur, P. C. Hammel, and F. Y. Yang, Phys. Rev. B **88**, 100406(R) (2013).
[11] C. H. Du, H. L. Wang, Y. Pu, T. L. Meyer, P. M. Woodward, F. Y. Yang, and P. C. Hammel, Phys. Rev. Lett. **111**, 247202 (2013).
[12] R. C. Linares, R. B. McGraw, and J. B. Schroeder, J. Appl. Phys. **36**, 2884 (1965).
[13] P. C. Dorsey, S. E. Bushnell, R. G. Seed, and C. Vittoria, J. Appl. Phys. **74**, 1242 (1993).
[14] S. A. Manuilov, R. Fors, S. I. Khartsev, and A. M. Grishin, J. Appl. Phys. **105**, 033917 (2009).
[15] Y. Sun, Y. Song, H. Chang, M. Kabatek, M. Jantz, W. Schneider, M. Wu, H. Schultheiss, and A. Hoffmann, Appl. Phys. Lett. **101**, 152405 (2012).
[16] R. Zeyfang, J. Appl. Phys. **41**, 3718 (1970).
[17] J. H. Collins, N. Rubino, H. R. Zapp, J. E. Mee, F. A. Pizzarello, G. R. Pulliam, and T. N. Hamilton, Appl. Phys. Lett. **13**, 93 (1968).
[18] A. J. Hauser, R. E. A. Williams, R. A. Ricciardo, A. Genc, M. Dixit, J. M. Lucy, P. M. Woodward, H. L. Fraser, and F. Y. Yang, Phys. Rev. B **83**, 014407 (2011).
[19] A. J. Hauser, J. R. Soliz, M. Dixit, R. E. A. Williams, M. A. Susner, B. Peters, L. M. Mier, T. L. Gustafson, M. D. Sumption, H. L. Fraser, P. M. Woodward, and F. Y. Yang, Phys. Rev. B **85**, 161201(R) (2012).
[20] X. Liu, W. L. Lim, L. V. Titova, M. Dobrowolska, J. K. Furdyna, M. Kutrowski, and T. Wojtowicz, J. Appl. Phys. **98**, 063904 (2005).
[21] M. Farley, Rep. Prog. Phys. **61**, 755 (1998).
[22] P. Hansen, P. Röschmann, and W. Tolksdorf, J. Appl. Phys. **45**, 2728 (1974).
[23] H. Suhl, Phys. Rev. **97**, 555 (1955).
[24] Y. Q. He and P. E. Wigen, J. Magn. Magn. Mater. **53**, 115 (1985).
[25] X. Liu, Y. Sasaki, and J. K. Furdyna, Phys. Rev. B **67**, 205204 (2003).
[26] J. J. Krebs, B. T. Jonker, and G. A. Prinz, J. Appl. Phys. **61**, 2596 (1987).
[27] F. Y. Yang, C. H. Shang, C. L. Chien, T. Ambrose, J. J. Krebs, G. A. Prinz, V. I. Nikitenko, V. S. Gornakov, A. J. Shapiro, and R. D. Shull, Phys. Rev. B **65**, 174410 (2002).
[28] B. Peters, A. Alfonsov, C. G. F. Blum, S. J. Hageman, P. M. Woodward, S. Wurmehl, B. Büchner, and F. Y. Yang, Appl. Phys. Lett. **103**, 162404 (2013).
[29] C. Chappert and P. Bruno, J. Appl. Phys. **64**, 5736 (1988).
[30] R. Zuberek, K. Fronc, A. Szewczyk, and H. Szymczak, J. Magn. Magn. Mater. **260**, 386 (2003).
[31] O. Mosendz, V. Vlaminck, J. E. Pearson, F. Y. Fradin, G. E. W. Bauer, S. D. Bader, and A. Hoffmann, Phys. Rev. B **82**, 214403 (2010).
[32] E. Shikoh, K. Ando, K. Kubo, E. Saitoh, T. Shinjo, and M. Shiraishi, Phys. Rev. Lett. **110**, 127201 (2013).